LASER
& PHOTONICS
REVIEWS

Laser Photonics Rev. **9,** No. 5, 507–516 (2015) / **DOI** 10.1002/lpor.201500063

Abstract The newly engineered ternary CdZnS/ZnS colloidal quantum dots (CQDs) are found to exhibit remarkably high photoluminescence quantum yield and excellent optical gain properties. However, the underlying mechanisms, which could offer the guidelines for devising CQDs for optimized photonic devices, remain undisclosed. In this work, through comprehensive steady-state and time-resolved spectroscopy studies on a series of CdZnS-based CQDs, we unambiguously clarify that CdZnS-based CQDs are inherently superior optical gain media in the blue spectral range due to the slow Auger process and that the ultralow threshold stimulated emission is enabled by surface/interface engineering. Furthermore, external cavity-free high-Q quasitoroid microlasers were produced from self-assembly of CdZnS/ZnS CQDs by facile inkjet printing technique. Detailed spectroscopy analysis confirms the whispering gallery mode lasing mechanism of the quasitoroid microlasers. This tempting microlaser fabrication method should be applicable to other solution-processed gain materials, which could trigger broad research interests.

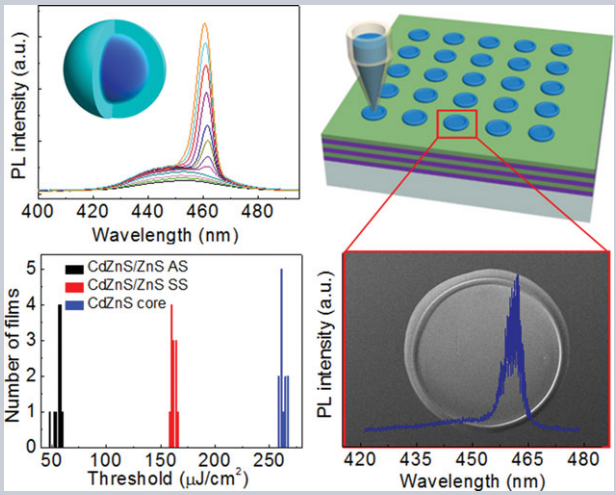

ORIGINAL PAPER

Unraveling the ultralow threshold stimulated emission from CdZnS/ZnS quantum dot and enabling high-Q microlasers

Yue Wang[1], Kah Ee Fong[2], Shancheng Yang[1], Van Duong Ta[1], Yuan Gao[1], Zeng Wang[1,3], Venkatram Nalla[3], Hilmi Volkan Demir[1,2,3,4,*], and Handong Sun[1,3,*]

1. Introduction

By virtue of the quantum confinement effect and solution processibility, colloidal quantum dots (CQDs) promise the most cost-effective photonic devices including light-emitting diodes (LEDs) and lasers covering the full visible spectral range [1–3]. However, the performance of blue CQD devices is always inferior to green and red counterparts due to the lack of applicable blue-emitting CQDs. Fabrication of blue binary CdSe-based CQDs with high photoluminescence quantum yield (PL QY) is not as facile as for red ones [4]. Furthermore, the reduced dot size of blue-emitting CdSe-based CQDs results in a much faster nonradiative Auger recombination (AR) rate under high excitation intensities [5–7], plaguing their optical gain in blue spectral range. Consequently, exploring suitable blue-emitting CQDs alternative to CdSe-based ones becomes imperative in view of developing efficient blue and full-visible color LEDs and lasers. Strikingly, the newly engineered ternary CdZnS/ZnS alloyed-core/shell CQDs have been found to show an unprecedented high PL QY of up to ~90% with wavelength tunable in the blue region (410–470 nm) [8, 9], and by far the best blue LEDs with a maximum luminance of 2624 cd/m^2 and external quantum efficiency of 7.1% have been realized based on these CQDs [8]. Very recently, we realized liquid blue lasers with ultralow thresholds by employing CdZnS/ZnS CQDs as the gain material [6, 10]. However, so far, the underlying mechanisms for the exceptionally high PL QY and the surprisingly low lasing threshold, which, in turn, can offer clues for designing CQDs for optimizing photonic devices, have not yet been explored. In this work, we present a comprehensive steady-state and time-resolved spectroscopy study on ternary CdZnS alloyed-cores (core), CdZnS/ZnS alloyed-core/sharp-shell (SS) and CdZnS/ZnS alloyed-core/alloyed-shell (AS) CQDs in an attempt to unravel the unknowns. It is unambiguously revealed that CdZnS-based CQDs are inherently superior gain media due to the slow AR, and we directly demonstrate the importance of surface/interface engineering to manipulate the

[1] Division of Physics and Applied Physics, School of Physical and Mathematical Sciences, Nanyang Technological University, Singapore 637371, Singapore
[2] School of Electrical and Electronic Engineering, Luminous! Center of Excellence for Semiconductor Lighting and Displays, Nanyang Technological University, Nanyang Avenue, Singapore 639798, Singapore
[3] Centre for Disruptive Photonic Technologies (CDPT), Nanyang Technological University, Singapore, Singapore 637371, Singapore
[4] Department of Electrical and Electronics Engineering, Department of Physics, and UNAM-National Nanotechnology Research Center, Bilkent University, Bilkent, Ankara, Turkey
*Corresponding author: e-mail: HDSun@ntu.edu.sg and HVDemir@ntu.edu.sg

gain properties of CQDs [8]. The combination of the intrinsic superb gain property of ternary alloy CdZnS-based CQDs and the interface-alloying effect leads to the ultralow threshold stimulated emission from CdZnS/ZnS AS CQDs. Furthermore, leveraging on these optimized CdZnS/ZnS AS CQDs, we, for the first time, achieved three-photon-pumped stimulated emission from CQDs in the blue spectral range.

Up till now, CQD-based lasers are typically fabricated by doping CQDs into or coating onto different kinds of external resonators [2, 6, 11–13], and only a few external cavity-free CQD lasers [14–16], in which the CQDs behave as both the gain media and the resonator [17], have been reported. Herein, we realized external cavity-free high-Q quasitoroid microlasers from self-assembly of CdZnS/ZnS AS CQDs by a facile one-step inkjet printing method [18], where the optical feedback is provided by the total internal reflection occurring at the surface of the ring wall formed by the coffee-stain effect [19]. This attractive microlaser fabrication method should be applicable to other solution-processed gain materials, which will draw widespread research attention. Overall, our results shed light on designing high-quality CQDs for low-threshold lasers and present a novel tempting fabrication method towards fascinating CQD lasers, besides providing the insightful physical mechanisms.

2. Experimental materials and methods

CdZnS core, CdZnS/ZnS SS and CdZnS/ZnS AS CQDs are fabricated using a one-pot method [8, 9]. To produce CdZnS/ZnS SS CQDs, limited shell formation time (20 min) is allowed following second injection of the sulfur precursor. In contrast, to produce CdZnS/ZnS AS CQDs, an additional high temperature (310 °C) annealing process is applied. In brief, the solution of cadmium and zinc oleate was first acquired from a stirring mixture of 128.4 mg (1 mmol) of cadmium oxide, 1.8349 g (10 mmol) of zinc acetate and 9.5 mL (30 mmol) of oleic acid, which were heated to 150 °C under vacuum in a 3-necked 50 mL round-bottom flask. Subsequently, 12.5 mL noncoordinating solvent of octadecene (ODE) was added and the air as well as the moisture were removed. Then, the solution was heated to 310 °C under inert gas, and 51.3 mg (1.6 mmol) of sulfur powder predissolved in 2.4 mL of ODE was swiftly injected into the hot solution to initiate the nucleation. The reaction was held for 12 min before cooling to a temperature of ∼70 °C. To fabricate CdZnS/ZnS SS CQDs, 128.3 mg (4 mmol) of sulfur powder predissolved in 5 mL of oleic acid was injected in a dropwise manner into the flask to grow ZnS shell. The reaction was held for 20 min followed by rapid cooling to a temperature ∼70 °C. To fabricate CdZnS/ZnS AS CQDs, the ZnS shell was grown on by the same procedures as for CdZnS/ZnS SS CQDs but with a further annealing process for 3 h at 310 °C. All these nanocrystals were purified by repeated acetone/methanol precipitation and toluene redispersion, and the final CQDs solutions was kept at 4 °C in the dark until further use.

For the time-resolved PL measurements, the CQDs solution filled in quartz cuvettes with a thickness of 1 mm was excited at 400 nm. The pulse-width and repetition rate are 100 fs and 1000 Hz, respectively. The PL signals were recorded by an Optronis streak camera with a temporal resolution of ∼50 ps. For the stimulated emission investigation, a femtosecond amplified laser system with wavelength tunable from 260 to 2600 nm was employed as the excitation source. The laser beam was focused by a cylinder lens (focus length: 75 mm) onto the samples with dimensions of ∼100 μm × 5 mm. The PL signals from the edge of the samples are dispersed by a 320-mm monochromator and detected by a silicon charged coupled device (CCD). In doing micro-PL (μ-PL) measurements, the laser beam offering laser pulses with an optical wavelength of 400 nm, pulse-width of 5 ns and repetition rate of 20 Hz was guided and focused to an elliptical spot with dimensions of ∼300 × 400 μm^2, and the emission signal was collected by a microscope objective (NA: 0.42, 50X) combined with suitable filters and detected by a silicon CCD.

3. Results and discussions

3.1. Steady-state and time-resolved spectroscopy on CdZnS core, CdZnS/ZnS SS and CdZnS/ZnS AS CQDs

The atomic percentages of Cd and Zn in CdZnS core were extracted by energy-dispersive X-ray (EDX) measurements as ∼22% and ∼28% (Fig. S1), respectively. To confirm the shell formation in CdZnS/ZnS SS CQDs and the interface alloying in CdZnS/ZnS AS CQDs during the annealing process, which are expected to influence the electronic structures and change the optical transition probability and energy, we carried out steady-state absorption and PL measurements for elucidation. Figure 1a shows the absorption spectra of CdZnS core, CdZnS/ZnS SS and CdZnS/ZnS AS CQDs in solution. The gradually increased absorption at higher energy of CdZnS/ZnS SS and CdZnS/ZnS AS CQDs with respect to CdZnS core originates from the absorption of the ZnS shell [4, 10], which indicates the success in shell formation for CdZnS/ZnS SS CQDs and that the shell thickness grows during the annealing process. According to the transmission electron microscopy (TEM), the sizes of the CdZnS core, CdZnS/ZnS SS and CdZnS/ZnS AS CQDs are measured to be 6.8, 9.4 and 11.4 nm, which further confirms shell formation (∼4 monolayers of ZnS) [8] for CdZnS/ZnS SS CQDs and the increase of shell thickness for CdZnS/ZnS AS CQDs during the annealing process. It is worth noting that large shell thickness is always preferred in view of enhancing the photostability of CQDs. However, the PL QY tends to rapidly decrease with increase of shell thickness after certain value due to defect formation arising from the release of stress existing in core–shell interface [8, 20], which, however, is opposite

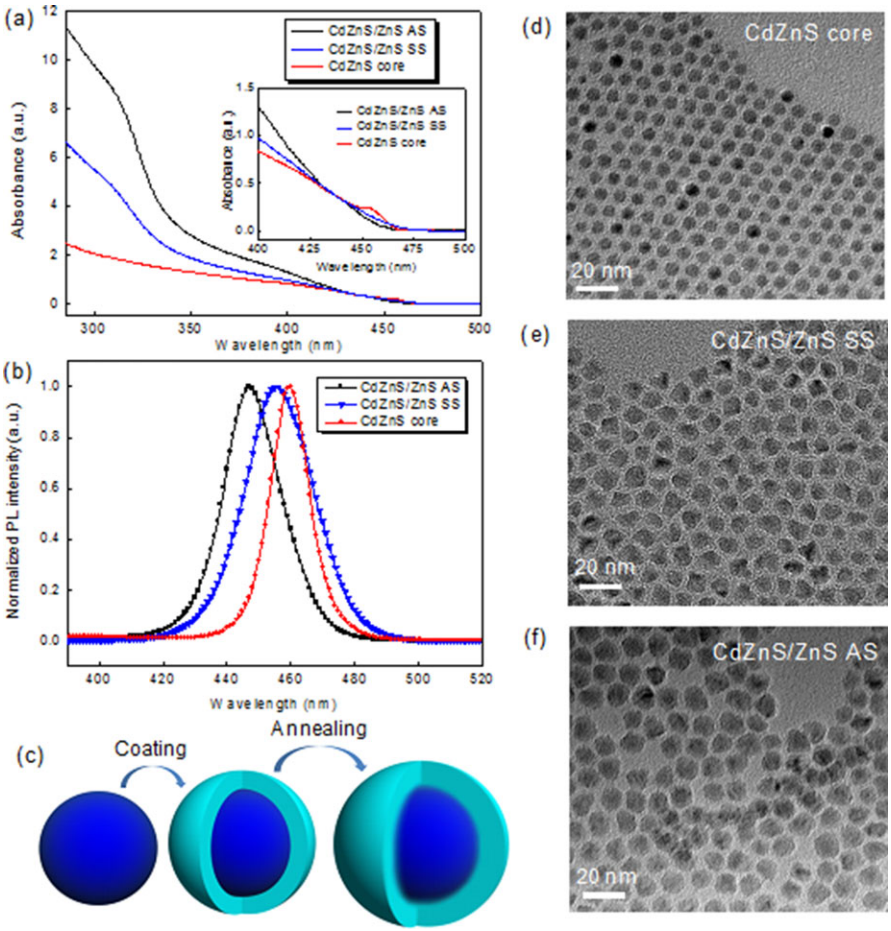

Figure 1 Absorption (a) and emission (b) spectra of CdZnS core, CdZnS/ZnS SS and CdZnS/ZnS AS CQDs. The inset in (a) shows the zoom-in of absorption spectra near the band edge. (c) Schematic structure of CdZnS core, CdZnS/ZnS SS and CdZnS/ZnS AS CQDs from left to right, respectively. TEM images of CdZnS core (d), CdZnS/ZnS SS (e) and CdZnS/ZnS AS CQDs (f).

to our case (detailed discussion will be shown later). The zoom-in of absorption spectra (Fig. 1a, inset) near the band edge reveals a blueshift of CdZnS/ZnS AS CQDs compared to CdZnS/ZnS SS CQDs. This result verifies the interdiffusion of the Zn ion in the shell and the Cd ion in the core during the annealing process [8, 10], which is further evidenced by the high-resolution TEM measurements (Fig. S2), thus confirming the alloying of the interface [8, 10, 21]. The schematic structures of CdZnS core, CdZnS/ZnS SS and CdZnS/ZnS AS CQDs are portrayed in Fig. 1c. In addition, we observed the smearing out of the band-edge exciton absorption peak of CdZnS/ZnS SS and CdZnS/ZnS AS CQDs compared to CdZnS core, indicating the increased inhomogeneity in size or composition, which is consistent with the PL linewidth variation of the samples (14 nm, 21 nm and 19 nm for CdZnS core, CdZnS/ZnS SS and CdZnS/ZnS AS CQDs, respectively). Importantly, the PL QY increases from ~10% for CdZnS core to ~47% after shell formation and reaches ~90% for the exceptional large-sized CdZnS/ZnS AS CQDs with an effective shell thickness of ~7.5 monolayers of ZnS, which is in stark contrast to the conventional CQDs, such as CdSe/CdS CQDs, where the PL QY for those with such large shell thicknesses is usually quite low [20, 22]. It is known that generally the poor PL QY originates from nonradiative recombination associated with surface/interface defects [23–25]. In our case, the shell formation can effectively passivate the surface defects, thus increasing the PL QY. However, due to the lattice mismatch between the Cd-rich core and the ZnS shell, defects tend to form at the interface. During the annealing process, the sharp interface between the core and shell will get "soft" or alloyed owing to the interdiffusion of Zn ion. As a result, the interface defects could be released by the annealing process. To confirm the above explanation, temperature-dependent PL measurements were performed on our samples (Figs. 2a–c). The integrated PL intensities as a function of temperature (10–300 K) are presented in Fig. 2d. It can be seen that the PL intensity of CdZnS cores decreases rapidly with increasing temperature, and it maintains only 8.5% of the initial (10 K) PL intensity at room temperature. In contrast, CdZnS/ZnS SS CQDs are able to maintain 36% of the initial PL intensity, and CdZnS/ZnS AS CQDs can sustain as much as 82%. It is well known that surface/interface defects can serve as the carrier trapping centers at higher temperatures, preventing the radiative recombination and reducing the PL intensity [26]. In turn, preservation of PL intensity with increased temperature suggests the reduction of surface/interface defects [6, 26]. The appearance of defect-state emission at ~620 nm for CdZnS core and that only band-edge emission was observed for CdZnS/ZnS SS and CdZnS/ZnS AS CQDs (see insets in Figs. 2a–c) at low temperature (10 K) further confirms

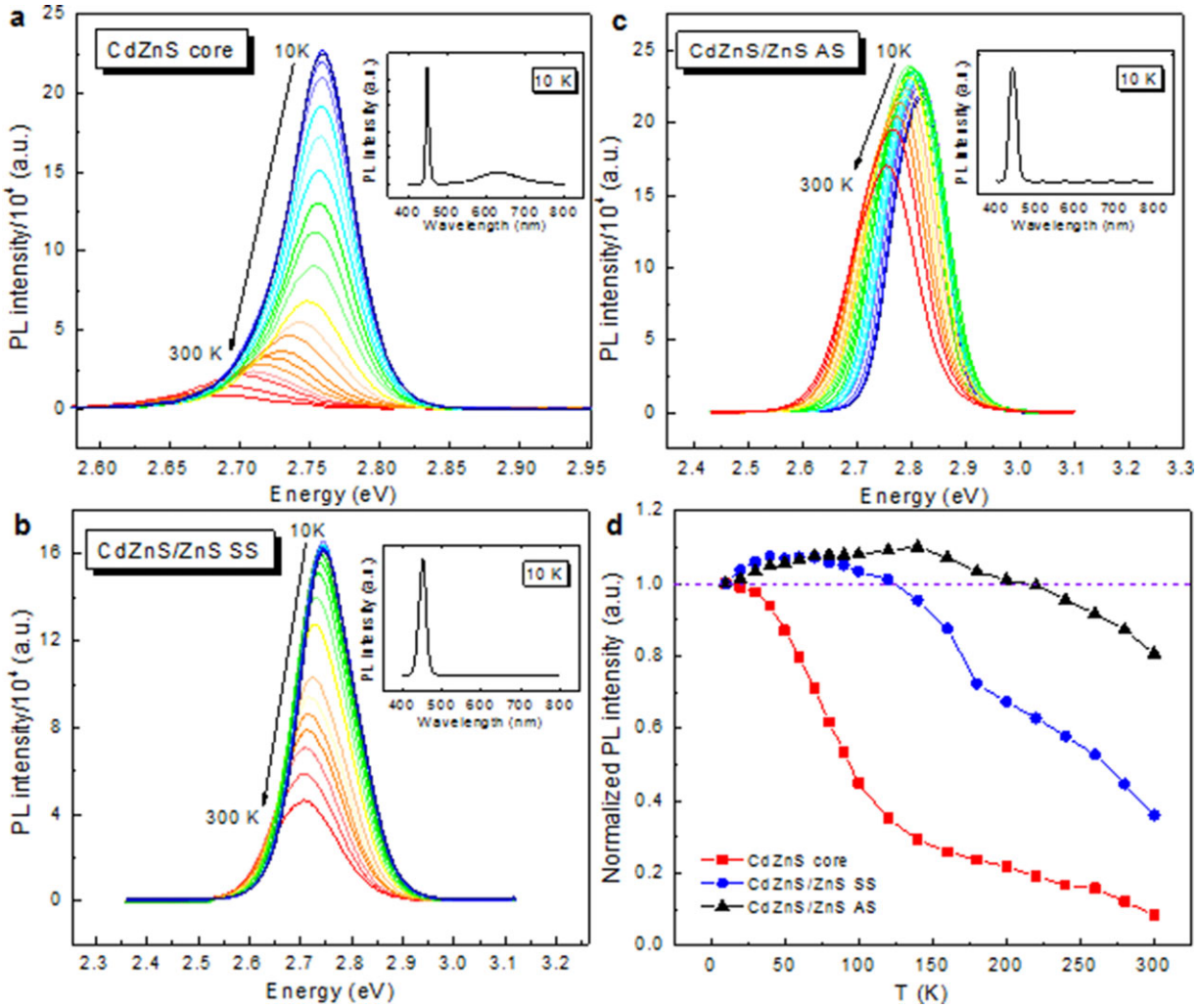

Figure 2 Tempearture-dependent PL spectra of CdZnS core (a), CdZnS/ZnS SS (b) and CdZnS/ZnS AS CQDs (c). The PL intensity of CdZnS core shows a monotonic decrease as the temperature increases, while those for CdZnS/ZnS SS and CdZnS/ZnS AS QDs exhibit antiquenching behavior at the early heating stage and then decrease with further increase of temperature. The insets shows PL spectra at 10 K for a broad wavelength range. (d) Temperature-dependent spectrally integrated PL intensity of CdZnS core, CdZnS/ZnS SS and CdZnS/ZnS AS CQDs.

the suppression of the surface/interface defects. Noticeably, differing from the CdZnS core whose PL intensity shows a monotonic decrease with increasing temperature, the PL intensities of CdZnS/ZnS SS and CdZnS/ZnS AS CQDs display an antiquenching behavior at the beginning of the heating stage and subsequently start decreasing. This phenomenon can be attributed to the competition between the thermal release of shallowly localized carriers at the interfaces into the CdZnS core that contribute to the increase of the PL intensity and the carrier trapping by the residual deep-level surface/interface defects or the nonradiative thermal escape of carriers assisted by multiphonon [26,27]. In addition, the PL intensity of CdZnS/ZnS SS CQDs increases faster and reaches its maximum earlier than that of CdZnS/ZnS AS CQDs (∼50 K and ∼150 K for CdZnS/ZnS SS and CdZnS/ZnS AS CQDs, respectively), indicating that more excited carriers are localized at the surface/interface of CdZnS/ZnS SS CQDs and thus more surface/interface defects exist in CdZnS/ZnS SS CQDs [26]. In order to access the PL dynamics that would give more information about the photophysical properties of CQDs, we performed the time-resolved spectroscopy. Figure 3a presents the PL decay traces of our samples monitored at peak wavelengths under low excitation intensity (∼12 μJ/cm^2), corresponding to the single-exciton regime. Obviously, there is a rapid decay process for CdZnS core, which is ascribed to the carrier-trapping effect [22, 28]. This rapid process is suppressed dramatically in CdZnS/ZnS SS CQDs and is even undetectable in CdZnS/ZnS AS CQDs, again indicating that the shell formation can effectively passivate the surface defects and the annealing process could optimize it, which is consistent with the temperature-dependent PL investigation. Note that the high PL QY (∼90% for CdZnS/ZnS AS CQDs) indicates low optical loss, which is beneficial for the achievement of stimulated emission and lasing.

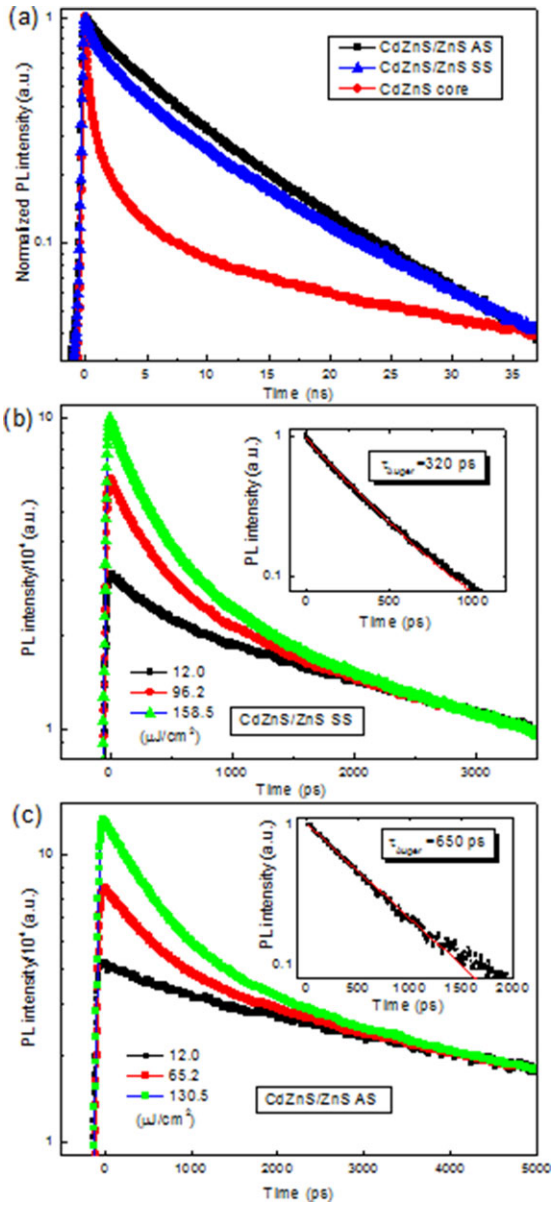

Figure 3 (a) PL decay dynamics of CdZnS core, CdZnS/ZnS SS and CdZnS/ZnS AS CQDs under low excitation intensity. Excitation intensity dependent PL decay dynamics of CdZnS/ZnS SS (b) and CdZnS/ZnS AS CQDs (c). The insets shows the extracted Auger lifetimes of CdZnS/ZnS SS (~320 ps) and CdZnS/ZnS AS CQDs (~650 ps) using a subtraction procedure.

3.2. Achieving ultralow threshold stimulated emission and unraveling the underlying mechanisms

Klimov and coworkers have demonstrated that the interfacial alloying could dramatically affect the multiexciton decay process or nonradiative AR for CdSe/CdS CQDs despite the fact that it has little influence on the single-exciton lifetime [21]. Naturally, we anticipate similar effect in our blue-emitting CdZnS/ZnS CQD system. Figures 3b and c illustrate the exciton dynamics of CdZnS/ZnS SS and CdZnS/ZnS AS CQDs under varied excitation intensities. An obvious fast decay process manifests with the increase of excitation intensities, which corresponds to the nonradiative AR [6, 22]. The Auger lifetime is derived to be ~320 ps for CdZnS/ZnS SS CQDs by adopting the subtraction procedure (inset of Fig. 3b) [21, 22], while that for CdZnS/ZnS AS CQDs is determined to be ~650 ps (inset of Fig. 3c), which is even longer than those of the red-emitting CQDs [21, 22], indicating that the Auger process in CdZnS/ZnS CQDs can be controlled by interface manipulation. The much increased Auger lifetime of the CdZnS/ZnS AS CQDs compared to CdZnS/ZnS SS CQDs is mainly attributed to the gradient interface potential profile in CdZnS/ZnS AS CQDs due to the interface-alloying effect that will inhibit AR by more strict momentum conservations compared to the relatively steep interface potential existing in CdZnS/ZnS SS CQDs [29, 30]. The efficient carrier trapping in CdZnS core complicates the extraction of its Auger lifetime. Nevertheless, it is reasonable to assume that it has a similar AR rate to that of CdZnS/ZnS SS CQDs [31]. In fact, Auger lifetimes with a timescale of ~300 ps for CdZnS core and CdZnS/ZnS SS CQDs are already several tens of times longer than those of blue-emitting CdSe/ZnS CQDs. The inherent slow AR rate in CdZnS-based QDs stems from the large size of the CdZnS cores, leading to a reduced overlap between electron and hole wave functions compared to that in blue-emitting CdSe-based CQDs [5, 6, 31]. It is known that AR is the main optical loss under high excitation intensities, the intrinsic slow AR renders the CdZnS-based CQDs highly possible as the favored optical gain material in the blue spectral range, offsetting the shortage of CdSe-based CQDs. To investigate the stimulated emission properties of these CQDs, the close-packed films of these samples prepared by a spin-coating method were pumped using a stripe configuration [17]. A femtosecond amplified laser system offering laser pulses with a pulse-width of 100 fs, repetition rate of 1000 Hz and wavelength of 400 nm is employed as the pumping source. Figures 4a–c display the excitation-intensity-dependent PL spectra of CdZnS core, CdZnS/ZnS SS and CdZnS/ZnS AS CQDs, respectively. It is found that all of the samples could show spectral narrowing at high excitation intensities and the excitation-intensity dependence of the integrated intensities over the sharp peaks exhibits a threshold behavior that clearly confirms the occurrence of stimulated emission [5]. The redshifted stimulated emission peak compared to the corresponding spontaneous emission peak consists with the biexcitonic gian mechanism in these CdZnS/ZnS CQDs [6]. Notably, the CdZnS core with PL QY of ~10% represents the poorest surface quality and efficient carrier trapping [5]. However, it is still able to develop stimulated emission thanks to the intrinsic slow AR, which implys that the carrier-trapping effect is not the fatal obstacle to achieve stimulated emission or lasing for CQDs because the defect states will saturate under high excitation intensities [5]. Following surface passivation by the ZnS shell, the threshold could be reduced to some extent due to the alleviated trapping loss. Surprisingly, the threshold abruptly decreases to ~55 μJ/cm^2 for CdZnS/ZnS AS

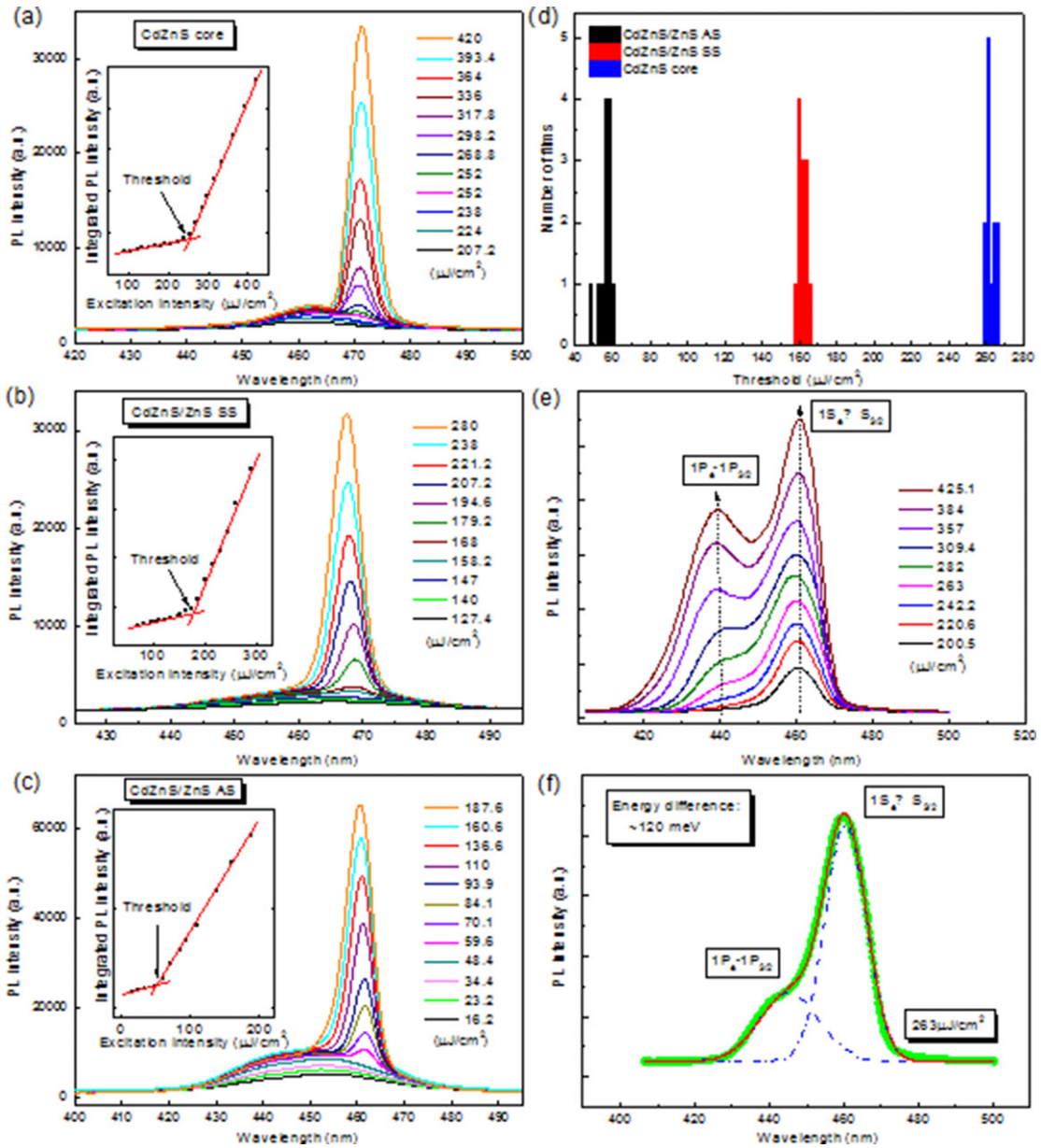

Figure 4 Stimulated emission of CdZnS core (a), CdZnS/ZnS SS (b) and CdZnS/ZnS AS CQDs (c) under an excitation wavelength of 400 nm. The insets shows the integrated PL intensity over the narrow peak as a function of excitation intensity. (d) Histogram of the stimulated emission thresholds for different films of CdZnS core, CdZnS/ZnS SS and CdZnS/ZnS AS CQDs. (e) Development of simultaneous two-state stimulated emission from CdZnS/ZnS AS CQDs. (f) Energy separation between $1S_e$–$1S_{3/2}$ and $1P_e$–$1P_{3/2}$ optical transitions.

CQDs, which is one order of magnitude lower than that of a recent report from unconventional pyramid-shaped CdSe/ZnCdS CQDs and comparable to those of the best red ones [2, 10]. The dramatically decreased threshold could be attributed to the interface-alloying effect, which reduces the optical gain loss by both suppressed AR and the minimized surface/interface trapping considering that the absorbance of CdZnS/ZnS AS CQDs only slightly increases compared with that of CdZnS/ZnS SS CQDs at 400 nm (Fig. S3) [17, 32]. The thresholds of CdZnS core, CdZnS/ZnS SS and CdZnS/ZnS AS CQDs are measured for dozens of films and are found to be reproducible with slight fluctuation, as shown in Fig. 4d, confirming the superb optical gain performance of CdZnS/ZnS AS CQDs with alloyed interface. These results represent the first direct experimental evidence for minimizing the stimuated emission threshold of CQDs by surface/interface manipulation and unambiguously highlight the importance of surface/interface engineering for the manipulation of the gain properties of CQDs.

Interestingly, as we keep increasing the excitation intensity after the development of stimultated emission from

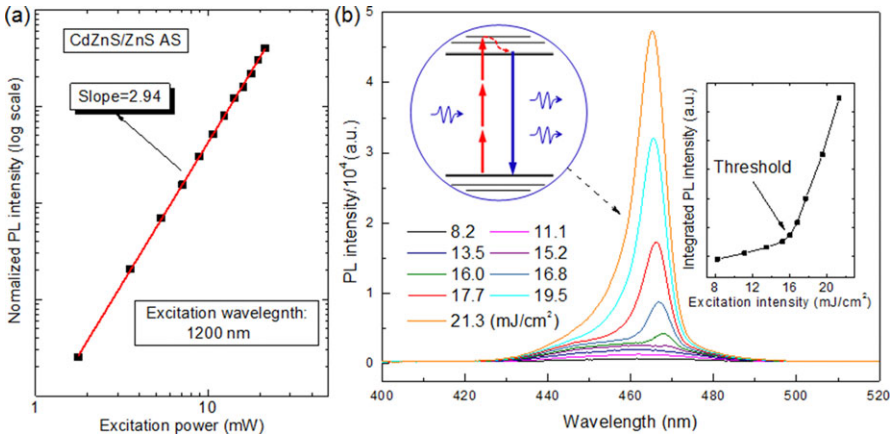

Figure 5 (a) Cubic dependence of integrated PL intensity on excitaiton intensity of CdZnS/ZnS AS CQDs under an excitation wavelength of 1200 nm. (b) Develeopment of stimulated emission by direct three-photon absorption. The right inset shows the integrated PL intensity over the narrow peak as a function of excitation intensity. The left inset shows the schematic stimulated emission process under three-photon pumping.

the $1S_{3/2}$–$1S_e$ optical transition, high-order multiexcitonic stimulated emission involving states of $1P_e$–$1P_{3/2}$ was observed from the CdZnS/ZnS AS CQDs with excitation intensity as low as 220 μJ/cm^2 (Fig. 4e), which is a direct reflection of slow AR in these CQDs. The simultaneous two-state stimulated emission spectra can be well reproduced by a Gaussian function with two peaks (Fig. 4f), from which the energy separation between $1P_{3/2}$–$1P_e$ and $1S_{3/2}$–$1S_e$ transitions is extracted to be ~120 meV.

3.3. Three-photon-induced stimulated emission in blue region

Three-photon pumping is strongly preferred in certain fields, especially biophotonics research and applications, due to the near-infrared excitation wavelength and high spatial resolution [17, 33]. By engineering CdSe/CdS/ZnS core–multishell CQDs, we have demonstrated three-photon-excited stimulated emission in the red regime [17]. Nevertheless, extending the stimulated emission wavelengths by three-photon absorption down to blue is extremely difficult. To explore the possibility of three-photon-induced stimulated emission from the optimized CdZnS/ZnS AS CQDs, we employed the stripe pumping configuration as was similarly used in single-photon examination but with an excitation wavelength of 1200 nm that locates far away from its absorption edge. To confirm the three-photon absorption and emission process under an excitation wavelength of 1200 nm, we performed power-dependent PL measurement. The nearly cubic dependence of the integrated PL intensity on the excitation power (Fig. 5a) validates the three-photon absorption and emission process [17,33]. As contrast experiments, we first investigated the possibility of three-photon-pumped stimulated emission from CdZnS core and CdZnS/ZnS SS CQDs. Neither of these two QDs was able to achieve stimulated emission before being damaged due to the insufficient optical robustness. While for CdZnS/ZnS AS CQDs, a sharp peak appears as the excitation intensity increases, similar to the case under one-photon pumping, indicating the achievement of frequency-upconverted stimulated emission (Fig. 5b). The plot of the integrated PL intensity over the sharp peak wavelength range shows an abrupt increase at a certain point (Fig. 5b, right inset), which unambiguously validates the development of three-photon-pumped stimulated emission from CdZnS/ZnS AS CQDs with a low threshold of ~16.0 mJ/cm^2, which is comparable to that of the red-emitting CdSe/CdS/ZnS CQDs [17]. This result represents the first observation of stimulated emission in the blue region by simultaneous three-photon absorption and should be attributed to the suppressed AR and enhanced photostability for CdZnS/ZnS AS CQDs. The corresponding schematic stimulated emission process under three-photon pumping is depicted in the left inset of Fig. 5b.

3.4. High-Q quasitoroid microlasers by inkjet-printing technique

Toroid lasers have attracted a great deal of attention thanks to the high Q-factor and small mode volume [18, 34], but they suffer from the complex and costly fabrication processes [18, 34]. Herein, we realized an external cavity-free quasitoroid microlaser from self-assembly of CdZnS/ZnS AS CQDs by a facile one-step inkjet printing method. To this end, the CQDs solution with a concentration of ~5 mg/mL was loaded into the inkjet nozzle by capillary force, then, the CQDs droplets were deposited onto the distributed Bragg reflector (DBR) substrate by the microplotter. The DBR substrate was fabricated by alternatively depositing 27 pairs of SiO_2 and TiO_2 layers on glass plate via electron beam evaporation, the transmission spectrum of the DBR substrate is presented in Fig. S4. After the evaporation of solvent, CQDs disks could be obtained, as is schematically illustrated in Fig. 6a. The position of the disks can be well controlled by the microplotter system and the sizes of the disks can be tuned by changing the inkjet nozzle outlet size (Fig. S5). Figure 6b shows the optical image of a typical array of CQDs disks of ~80 μm in diameter. Due to the coffee-stain effect [19], a ring wall is formed at the disk boundary, indicating a quasitoroid structure, which is well resolved by scanning electron microscopy (SEM) (Fig. 6c).

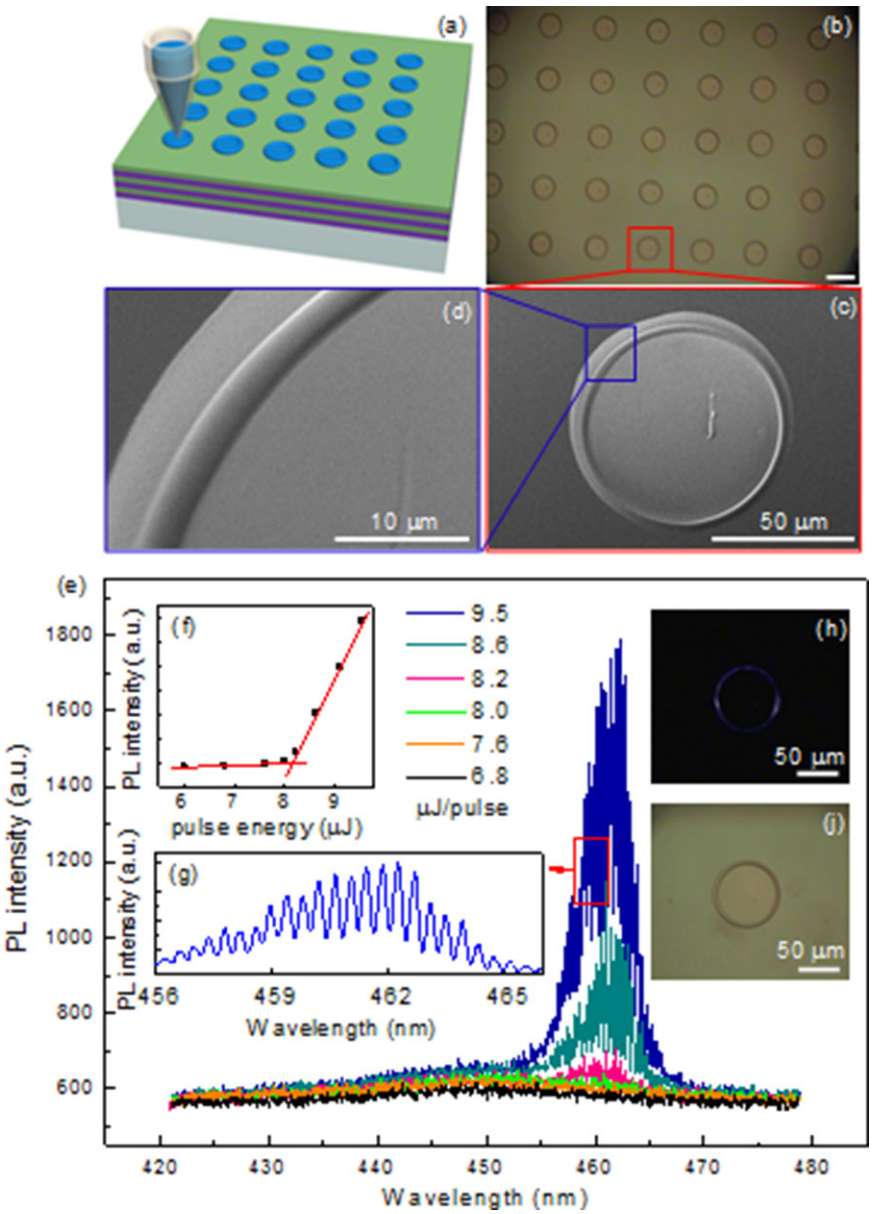

Figure 6 (a) Schematic illustration of inkjet method for the quasitoroid microlaser fabrication. (b) Optical image of a typical array of quasitoroid microlasers. Scale bar is 100 μm. (c) SEM image of a typical quasitoroid laser. (d) Higher-magnification SEM image of the ring wall area. (e) Power-dependent PL spectra of individual quasitoroid laser. (f) Integrated intensity of the lasing peaks as a function of excitation pulse energy. (g) Close-up of the lasing peaks in narrow wavelength range. (h) PL image of the quasitoroid laser above the lasing threshold. (j) Optical image of the quasitoroid microlaser.

The morphology and the cross-sectional profile of the ring wall was further investigated by atomic force microscopy (AFM), revealing a well-defined border of the ring wall (Fig. S6). This toroid-like structure is known to be more favorable than the traditional flat disk due to the better optical field confinement [18, 35, 36], hence a much higher Q-factor. Furthermore, the surface of the ring wall is found to be optically smooth (Fig. 6d and Fig. S6), which could effectively alleviate the scattering loss [37]. The optical investigation of the individual quasitoroid was conducted by using a home-built μ-PL system [36]. Figure 6e presents the μ-PL spectra from a typical quasitoroid of $\sim$80 μm (Fig. 6j) under various excitation energies. It is found that sharp discrete spikes with nearly equal interval (Figs. 6e and g), superimposing on the stimulated emission peak position, appear with the increase of the excitation energy, indicating the achievement of lasing action [17]. The plot of integrated PL intensity of the spikes as a function of excitation energy shows a nonlinear behavior (Fig. 6f), validating the development of lasing action with low threshold of $\sim$8.1 μJ/pulse or $\sim$6.7 mJ/cm^2 [5]. The Q-factor of the quasitoroid microlaser is determined to be as high as $\sim$2500 based on $Q = \lambda/\Delta\lambda$ [36], where λ and $\Delta\lambda$ are the wavelength and linewidth of the lasing peak, respectively, indicating the high quality of the quasitoroid microlaser. The ring-shaped emission pattern (Fig. 6h) above the lasing threshold consists of the conventional toroid lasing mechanism of whispering gallery mode (WGM) [38]. Based on the measured free spectral range (FSR) of the lasing spectra, the cavity length, L, can be derived, given by: FSR $= \lambda^2/nL$, where n is the refractive index of the QD disk. Assuming $n = 2$ [39], the cavity length is estimated to be $\sim$251 μm,

which approximately equals the circumference of the disk. Moreover, the FSR is found to be inversely proportional to the size of the quasitoroids (Fig. S7), further confirming the WGM mechanism of these quasitoroid microlasers [6, 18].

4. Conclusions and outlook

In conclusion, through a comprehensive optical study of a series of CdZnS-based CQDs by steady-state and time-resolved spectroscopy, the CdZnS-based CQDs are revealed to be intrinsically favored optical gain media in the blue region. Unambiguously, we demonstrate that optical gain properties of CQDs could be tailored by surface/interface engineering. The combination of the intrinsic superior gain property of CdZnS-based CQDs and the interface-alloying effect results in the ultralow threshold stimulated emission from CdZnS/ZnS alloyed-core/alloyed-shell CQDs. Interestingly, high-Q quasitoroid mirolasers were produced by a simple inkjet-printing technique. This fabrication method toward microlasers should also be applicable to other kinds of CQDs and similar solution-processible gain materials. Our results about the effects of surface/interface engineering on the gain properties of core–shell CQDs will shed light on developing low threshold laser materials based on quantum dots.

Supporting Information

Additional supporting information may be found in the online version of this article at the publisher's website.

Acknowledgments. This research is supported by the Singaporer National Research Foundation through the Competitive Research Programme (CRP) under Project No. NRFCRP6-2010-02, the Singapore Ministry of Education through the Academic Research Fund under Projects MOE 2011-T3-1-005 (Tier 3) and Merlion under Project. No. 2.02.

Received: 14 March 2015, **Revised:** 22 July 2015,
Accepted: 23 July 2015

Published online: 21 August 2015

Key words: CdZnS/ZnS quantum dots, Auger recombination, stimulated emission, multiphoton excitation, toroid laser.

References

[1] V. I. Klimov, Annu. Rev. Phys. Chem. **5**, 285–316 (2014).
[2] C. Dang, J. Lee, C. Breen, J. S. Steckel, S. Coe-Sullivan, and A. Nurmikko, Nature Nanotechnol. **7**, 335–339 (2012).
[3] B. Guzelturk, P. L. H. Martinez, Q. Zhang, Q. Xiong, H. Sun, X. W. Sun, A. O. Govorov, and H. V. Demir, Laser Photon. Rev. **8**, 73–93 (2014).
[4] W. K. Bae, M. K. Nam, K. Char, and S. Lee, Chem. Mater. **20**, 5307–5313 (2008).
[5] V. I. Klimov, A. A. Mikhailovsky, S. Xu, A. Malko, J. A. Hollingsworth, C. A. Leatherdale, H. J. Eisler, and M. G. Bawendi, Science **290**, 314–317 (2000).
[6] Y. Wang, K. S. Leck, T. Van Duong, R. Chen, V. Nalla, Y. Gao, T. He, H. V. Demir, and H. Sun, Adv. Mater. **27**, 169–175 (2015).
[7] Y. Chan, J. S. Steckel, P. T. Snee, J.-M. Caruge, J. M. Hodgkiss, D. G. Nocera, and M. G. Bawendi, Appl. Phys. Lett. **86**, 073102 (2005).
[8] K. H. Lee, J. H. Lee, W. S. Song, H. Ko, C. Lee, J. H. Lee, and H. Yang, ACS Nano **7**, 7295–7302 (2013).
[9] H. Shen, X. Bai, A. Wang, H. Wang, L. Qian, Y. Yang, A. Titov, J. Hyvonen, Y. Zheng, and L. S. Li, Adv. Funct. Mater. **24**, 2367–2373 (2014).
[10] B. Guzelturk, Y. Kelestemur, M. Z. Akgul, V. K. Sharma, and H. V. Demir, J. Phys. Chem. Lett. **5**, 2214–2218 (2014).
[11] F. Todescato, I. Fortunati, S. Gardin, E. Garbin, E. Collini, R. Bozio, J. J. Jasieniak, G. Della Giustina, G. Brusatin, S. Toffanin, and R. Signorini, Adv. Funct. Mater. **22**, 337–344 (2012).
[12] J. Q. Grim, S. Christodoulou, F. Di Stasio, R. Krahne, R. Cingolani, L. Manna, and I. Moreels, Nature Nano **9**, 891–895 (2014).
[13] P. T. Snee, Y. H. Chan, D. G. Nocera, and M. G. Bawendi, Adv. Mater. **17**, 1131–1136 (2005).
[14] Y. Chen, J. Herrnsdorf, B. Guilhabert, Y. Zhang, I. M. Watson, E. Gu, N. Laurand, and M. D. Dawson, Opt. Exp. **19**, 2996–3003 (2011).
[15] M. Zavelani-Rossi, R. Krahne, G. Della Valle, S. Longhi, I. R. Franchini, S. Girardo, F. Scotognella, D. Pisignano, L. Manna, G. Lanzani, and F. Tassone, Laser Photon. Rev. **6**, 678–683 (2012).
[16] F. D. Stasio, J. Q. Grim, V. Lesnyak, P. Rastogi, L. Manna, I. Moreels, and R. Krahne, Small **11**, 1328–1334 (2015).
[17] Y. Wang, T. V. Duong, Y. Gao, T. C. He, R. Chen, E. Mutlugun, H. V. Demir, and H. D. Sun, Adv. Mater. **26**, 2954–2961 (2014).
[18] D. K. Armani, T. J. Kippenberg, S. M. Spillane, and K. J. Vahala, Nature **421**, 925–928 (2003).
[19] M. Zavelani-Rossi, M. G. Lupo, R. Krahne, L. Manna, and G. Lanzani, Nanoscale **2**, 931–935 (2010).
[20] Y. Chen, J. Vela, H. Htoon, J. L. Casson, D. J. Werder, D. A. Bussian, V. I. Klimov, and J. A. Hollingsworth, J. Am. Chem. Soc. **130**, 5026–5027 (2008).
[21] W. K. Bae, L. A. Padilha, Y.-S. Park, H. McDaniel, I. Robel, J. M. Pietryga, and V. I. Klimov, ACS Nano **7**, 3411–3419 (2013).
[22] F. Garcia-Santamaria, Y. F. Chen, J. Vela, R. D. Schaller, J. A. Hollingsworth, and V. I. Klimov, Nano Lett. **9**, 3482–3488 (2009).
[23] D. D. Sarma, A. Nag, P. K. Santra, A. Kumar, S. Sapra, and P. Mahadevan, J. Phys. Chem. Lett. **1**, 2149–2153 (2010).
[24] J. D. Keene, J. R. McBride, N. J. Orfield, and S. J. Rosenthal, ACS Nano **8**, 10665–10673 (2014).
[25] H. Zhu, C. X. Shan, B. Yao, B.-H. Li, J. Y. Zhang, Z. Z. Zhang, D. X. Zhao, D. Z. Shen, X. W. Fan, Y. M. Lu, and Z. K. Tong, Adv. Mater. **21**, 1613–1617 (2009).
[26] P. Jing, J. Zheng, M. Ikezawa, X. Liu, S. Lv, X. Kong, J. Zhao, and Y. Masumoto, J. Phys. Chem. C **113**, 13545–13550 (2009).
[27] D. Valerini, A. Creti, M. Lomascolo, L. Manna, R. Cingolani, and M. Anni, Phys. Rev. B **71**, 235409 (2005).

[28] B. C. Fitzmorris, J. K. Cooper, J. Edberg, S. Gul, J. Guo, and J. Z. Zhang, J. Phys. Chem. C **116**, 25065–25073 (2012).
[29] G. E. Cragg and A. L. Efros, Nano Lett. **10**, 313–317 (2010).
[30] J. I. Climente, J. L. Movilla, and J. Planelles, Small **8**, 754–759 (2012).
[31] V. I. Klimov, A. A. Mikhailovsky, D. W. McBranch, C. A. Leatherdale, and M. G. Bawendi, Science **287**, 1011–1013 (2000).
[32] X. Wang, X. Ren, K. Kahen, M. A. Hahn, M. Rajeswaran, S. Maccagnano-Zacher, J. Silcox, G. E. Cragg, A. L. Efros, and T. D. Krauss, Nature **459**, 686–689 (2009).
[33] G. S. He, P. P. Markowicz, T. C. Lin, and P. N. Prasad, Nature **415**, 767–770 (2002).
[34] X. F. Jiang, Y. F. Xiao, C. L. Zou, L. He, C. H. Dong, B. B. Li, Y. Li, F. W. Sun, L. Yang, and Q. Gong, Adv. Mater. **24**, OP260–OP264 (2012).
[35] K. J. Vahala, Nature **424**, 839–846 (2003).
[36] R. Chen, B. Ling, X. W. Sun, and H. D. Sun, Adv. Mater. **23**, 2199–2204 (2011).
[37] K. H. Qing Liao, H. Zhang, X. Wang, J. Yao, and H. Fu, Adv. Mater. **7**, 133–139 (2015).
[38] B. Min, S. Kim, K. Okamoto, L. Yang, A. Scherer, H. Atwater, and K. Vahala, Appl. Phys. Lett. **89**, 191124 (2006).
[39] A. A. Ziabari and F. E. Ghodsi, Mater. Sci. Semicond. Process. **16**, 1629–1636 (2013).